Spectrum of Engineering Sciences
ISSN (e) 3007-3138 (p) 3007-312X
Volume 3, Issue 7, 2025

A COMPARATIVE FEM ANALYSIS OF DRAGON SKIN ELASTOMERS FOR OPTIMIZING SOFT PNEUMATIC ACTUATOR PERFORMANCE

Yumna Memon[*1], Saifullah Samo[2], Aamir Shaikh[3], Imran Ali Bhand[4], Safiullah Samo[5], Muhammad Ali Soomro[6]

[1,2,3,4,5,6]*Department of Mechatronic Engineering, Mehran University of Engineering & Technology, Jamshoro, Sindh, Pakistan*

[*1]myumna406@gmail.com, [2]saifullah.samo@faculty.muet.edu.pk, [3]aamir.shaikh@faculty.muet.edu.pk, [5]imranalibhand127@gmail.com, [4]safiullah.samo103@gmail.com, [6]soomro.ali@live.com

DOI: https://doi.org/10.5281/zenodo.15880968

Keywords
Soft Robotics, Soft Actuator, Bend angle, Finite Element Analysis, Soft Pneumatic Actuators, Hyperelastic Materials, Soft Grippers

Article History
Received: 02 April, 2025
Accepted: 23 June, 2025
Published: 08 July, 2025

Corresponding Author: *
Yumna Memon

Abstract
Soft pneumatic actuators are essential in soft robotics; their bending behavior depends on the non-linear characteristics of hyperelastic materials. Analytical models often cannot predict this performance accurately; computational techniques are needed for reliable results. The finite element method was used to quantitatively assess soft pneumatic actuators made from Dragon Skin 10 and Dragon Skin 30; both tested under the same pressurized loading. The research focused on understanding the trade-offs between achieving maximum bending and maintaining structural strength. Dragon Skin 10, which is more flexible, produced a maximum displacement of 0.161 m; Dragon Skin 30, which is stiffer, reached 0.092 m under identical conditions. Both materials experienced a peak von-Mises stress of about 1.37 x 10^5 Pa, showing that the stress response was similar regardless of flexibility. However, the greater bending of Dragon Skin 10 came with a much higher maximum equivalent strain of 0.565, while Dragon Skin 30 stayed at 0.204. These results highlight that using softer materials can increase actuator motion but brings the material closer to its strain threshold, which could affect durability. Conversely, stiffer materials like Dragon Skin 30 provide more structural strength and a larger margin of safety, making them better for applications that demand accuracy and long-term use. The findings present a practical framework for material selection in soft pneumatic actuator design, allowing engineers to match material properties with specific performance needs and application requirements. The study supports informed decision-making for optimizing soft robotic systems.

INTRODUCTION

Soft robotic systems have introduced a structural shift from rigid frameworks through improved compliance; adaptable deformation; and reduced physical risk during human-machine contact [1], [2]. Traditional rigid systems have been built using high-stiffness materials combined with discrete rotational joints; such designs frequently reduce mechanical flexibility and limit safe operation in sensitive or irregular environments. Soft robotic platforms instead employ materials that deform continuously; such materials support safer manipulation of fragile components and simplify access in confined or cluttered spaces [3], [4]. These mechanical benefits have expanded their usage into surgical tasks with low invasion levels [5]; biomedical tools for wearable or implantable functions [6]; and human-assisted assembly operations in shared workspaces [7] and remote operations in unstable or dangerous conditions [8]. Every system of this kind operates on a core element called the soft actuator; this element is responsible for producing force and displacement during motion [9], [10]. Among different actuation mechanisms, soft

pneumatic actuators (SPAs) have remained popular; they are favored due to high force-to-weight ratios; relatively low production cost; and simplified fabrication procedures [11], [12]. SPAs are pressurized through internal air-filled chambers embedded within a flexible body; as pressure increases, the actuator deforms in a programmable way through extension; torsion; or bending [13]. The actuator's physical behavior is dependent on the mechanical characteristics of the elastomer used; hyperelastic materials such as silicone are widely applied due to their high stretch limits and adjustable stiffness properties [14], [15]. A key challenge lies in the material's stress-strain relationship; this relationship behaves non-linearly under loading; such non-linearity complicates design and analytical formulation [16]. Classical mechanics methods rarely provide agreement between theoretical models and actual test results; particularly during large deformations and high strain conditions [17]. For this reason, computational modeling tools such as the Finite Element Method (FEM) are used; these tools enable accurate representation of deformation responses across varying geometries and materials [18], [19]. FEM-based simulations provide high-resolution prediction of shape changes under pressure; they also account for hyperelastic behavior not captured by simplified equations [20]. This research applies FEM simulations to evaluate two frequently used elastomers: Dragon Skin 10 and Dragon Skin 30; these materials differ mainly in stiffness. The objective is to quantify changes in actuator bending and mechanical strength as a function of material selection; results are intended to offer data-supported guidance during the SPA design process [21], [22].

The motion mechanism in SPAs operates based on the strain behavior of hyperelastic elastomers; such materials allow elastic stretch beyond typical limits without residual damage or permanent deformation [23], [24]. FEM simulations require specific strain energy density models to describe this behavior; commonly applied examples include the Neo-Hookean; Mooney-Rivlin; and Ogden models [25], [26]. These models are critical when simulating the curved deformation of SPAs under pneumatic loading. Bending deformation is introduced by design features such as embedded passive layers or geometric asymmetry; these techniques control where expansion occurs during actuation [27], [28]. When internal air chambers are filled, stiffer or restricted regions resist expansion; surrounding material then expands disproportionately; this imbalance creates bending forces that deflect the actuator [29], [30]. The level of bending observed is driven by internal pressure; geometry of the actuator; and material elasticity properties; key among these is Young's modulus and the hyperelastic parameters defining the constitutive model [31]. Softer materials tend to deflect more under the same pressure; this leads to higher bending angles but also increases internal stress levels. These stress levels may push the material close to rupture or yield thresholds; such outcomes negatively affect performance consistency and long-term reliability [32]. Achieving an optimal design therefore involves balancing flexibility against mechanical endurance; this relationship is governed by the selected elastomer and geometric form [33].

Research in soft pneumatic actuator design has progressed across several areas; early investigations demonstrated actuator motion through air-driven inflation of elastomer chambers; these studies introduced the foundational concept of controllable deformation in soft bodies [34], [35]. Later studies expanded actuator design ranges by implementing geometric constraints such as fibers; these fibers restricted radial swelling while permitting axial elongation and increased curvature [36]. Other designs included bellow-type actuators; these units enabled translational motion with defined stroke limits and reduced lateral drift [37]. FEM became a widely used approach across many such studies; it was applied to determine optimal structural shapes; improve actuator force output predictions; and correlate numerical models with laboratory testing [38], [39], [40]. Investigations have also analyzed different elastomeric material types; comparisons have included silicone blends and hydrogel compounds; in some cases, materials were chosen for specialty functions including biocompatibility or repairability [41], [42]. Much of this work has emphasized custom-built actuator models; efforts have focused on novel structure geometries and unique material chemistries [43], [44]. A clear shortage remains in studies that directly compare commercial silicone materials using the same actuator geometry; few publications present side-by-side data on widely available options such as Dragon Skin products. Specific differences in Shore hardness, such as the variation between grades 10A and 30A, have not

been well characterized under standardized tests [45]. Bending response and peak strain are not often measured together in existing studies; this omission limits data-driven decisions regarding elastomer trade-offs during design. Therefore, comparative studies focusing on commercially accessible materials and controlled design parameters are needed; these can clarify how material selection affects performance metrics including bend angle and strain risk over repeated cycles.

Material selection remains the main challenge during soft pneumatic actuator (SPA) design; engineers must weigh opposing requirements that influence function and durability [46]. Softer elastomers such as Dragon Skin 10 offer a greater range of motion and increased bending angles under relatively low internal pressures; these features benefit robotic tasks that demand adaptability and fine control [47]. Stiffer materials such as Dragon Skin 30 provide higher load capacity and improved shape retention; these characteristics support repeatable positioning and prevent unwanted bulging or rupture under pressure [48]. Existing design procedures are often guided by past experience or time-consuming iterative testing; direct data comparing these two elastomers within the same actuator geometry remain uncommon in published research [49]. Well-established hyperelastic models already exist to represent silicone-based elastomers under large strain; examples include the Mooney-Rivlin and Neo-Hookean formulations [50]. Still, these models have not yet been widely applied to generate practical engineering comparisons between common grades of off-the-shelf silicone rubber using unified FEM simulation [51]. This research therefore focuses on a key question: How does the change in stiffness between Dragon Skin 10 and Dragon Skin 30 influence maximum bending displacement, internal von Mises stress, and equivalent strain in a soft pneumatic actuator exposed to the same input pressure? Addressing this question will provide a structured method to support actuator material decisions based on required performance outcomes rather than informal selection rules [52].

This study aims to deliver a direct and measurable comparison between Dragon Skin 10 and Dragon Skin 30 used in the same SPA configuration. The first objective is to generate high-accuracy finite element models using non-linear solvers; these models will be based on identical actuator geometries and incorporate verified hyperelastic material parameters. The second task is to conduct simulations that apply progressive pneumatic pressure; internal deformation responses will be tracked under matching load steps. The third goal is to extract and compare three major metrics from both models; the output will include maximum bending angles, von Mises stress distribution maps, and principal equivalent strain values. The final objective is to compile these results into a visual and written comparison that engineers can reference; this framework will describe mechanical trade-offs based on stiffness and provide evidence to support the elastomer selection in similar applications.

This work introduces a structured reference that connects material stiffness with actuator function using clear numerical evidence. Engineers designing soft robots will benefit from reduced reliance on manual testing; design loops will shorten because predicted deformation and stress results will support direct elastomer choices [53], [54]. The relationship between flexibility, bending, and strain will be presented in practical terms; these results will allow robotic designs to meet safety and motion requirements while maintaining strength and stability [55]. Application domains including assistive devices and human-safe interfaces will benefit directly; these areas often demand both soft contact and long operational life [56]. The proposed data-based workflow supports faster decision-making during material selection and increases confidence during design optimization for future soft robotic systems [57].

I. 3D CAD MODEL OF SOFT PNEMUMATIC ACTUATOR

The soft pneumatic actuator was designed using SolidWorks, a design and CAD software. The dimensions of the actuator, including its length, width, and height, were taken from the literature [58]. However, the chambers were designed with the aim of achieving optimal bending and minimizing stress level at low pressure. Figure 1 presents different views of the corrugated soft actuator, which displays various perspectives of the actuator, including its top view and isometric view.

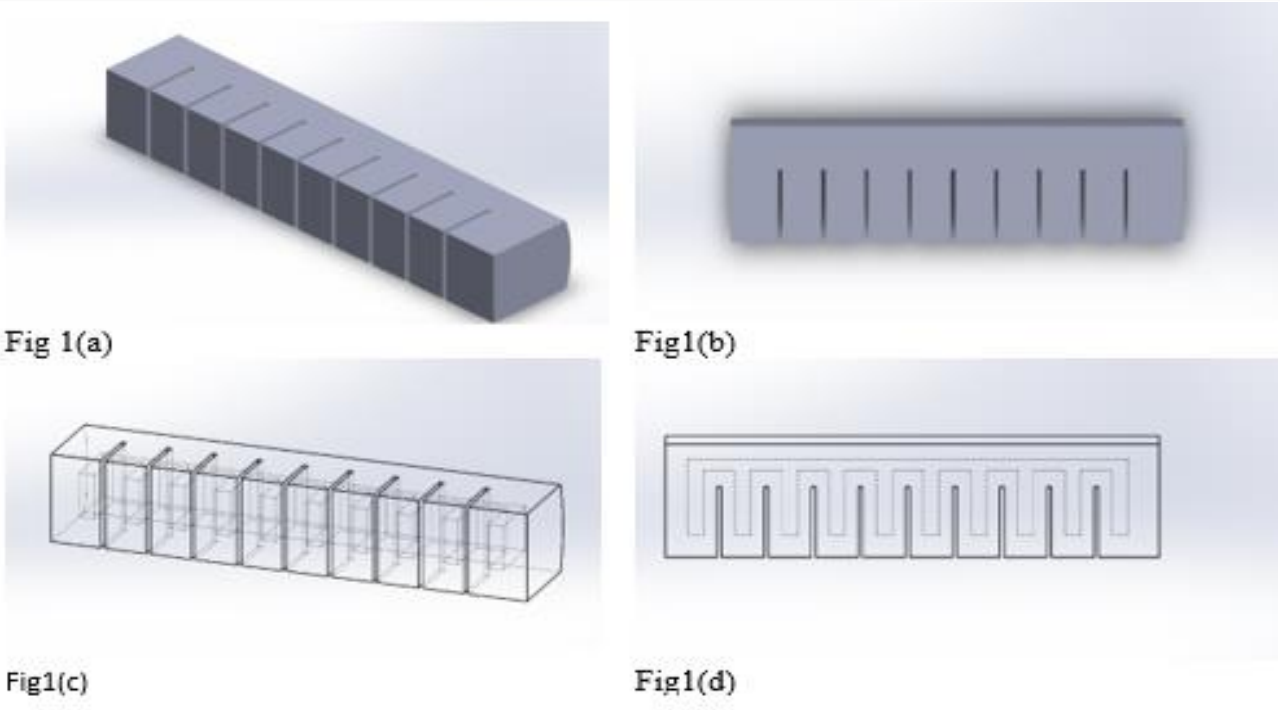

Figure 1. 3D Model of Soft Pneumatic Actuator.

Table 1. The parameters listed below are important in determining the performance of the soft actuator.

Parameters	Explanation	Dimensions(mm)
Length of soft actuator (L)	The distance between the two ends of the soft actuator. This determines the extent to which the actuator can extend and contract.	120
Height of soft actuator (H)	The height of the rectangular shape of the actuator.	19
Width of soft actuator (W)	The width of the actuator, which determines the amount of force it can exert.	20
Length of air pipe	The length of the pipe that supplies air to the actuator.	116
Width of air pipe	The diameter of the pipe that supplies air to the actuator.	2

.

II. SELECTION OF MATERIAL

The choice of silicone rubber as the actuator material was based on several factors, including its low cost, ease of molding into various shapes, and desirable properties for the actuator. It is crucial to select a material with reasonable stiffness that provides an adequate bending angle and blocking force for performing grasping tasks for soft robotic gripper applications. Furthermore, the potential for pneumatic channels should be considered when selecting materials. Various methods can be employed for evaluating the mechanical measurement of soft materials. Sylgard 184; Smooth-Sil 950; and Ecoflex 00-30 were previously measured to evaluate their material properties in soft robotic systems [59]. Soft actuators refer to elastomeric materials that deform and change shape under external forces such as electric; magnetic; or pneumatic pressure. These deformable materials are used in several engineering systems; including prosthetics; wearable electronics; and robotic devices. Dragon Skin 10 [60]; and Dragon Skin 30 [21]; are commercially available silicone rubbers that may serve as candidate materials for soft actuator construction. The present study conducts a comparative material evaluation between Dragon Skin 10 and Dragon Skin 30 for deformation-based applications. Dragon Skin 10 is often selected where high compliance is required due to its lower Shore A hardness value of 10. This lower hardness improves the actuator's ability to deform

under minimal applied stress; which supports its use in wearable or assistive applications. The material's flowability; low viscosity; and simple mixing ratio allow for precise mold filling; particularly in cases involving detailed and miniaturized parts. Dragon Skin 30 provides improved stiffness and mechanical stability; but Dragon Skin 10 remains the preferred choice where greater flexibility and ease of fabrication are required [10]. Dragon Skin 10 also displays favorable mechanical performance through high elongation at break and strong tear resistance, which supports its resistance to shape loss under repeated cyclic deformation. These characteristics make it a dependable candidate in devices requiring long-term mechanical endurance and repeatable motion performance.

III. SELECTION OF HYPER ELASTIC MATERIAL MODEL

Hyperelastic material models have been applied to describe elastomers that can tolerate large deformation without undergoing permanent shape change or material failure. Linear elastic models are not suitable when materials experience high strain levels beyond their elastic limit. Hyperelastic models define stress-strain responses that are nonlinear and commonly assume material incompressibility during deformation [40]. Neo-Hookean; Mooney-Rivlin; Ogden; and Yeoh models have been widely accepted for predicting the behavior of incompressible and elastic materials. Material constants in these models are usually obtained through curve fitting of experimental stress-strain data recorded from uniaxial or multiaxial tests. The Yeoh model has been used effectively for high-strain simulations where strain magnitudes exceed 400% and can extend to 1000% [40], [61]. The model shows strong predictive capability for multiple deformation types using only uniaxial test data as input. This feature has made the Yeoh model practical for modeling elastomers in various mechanical setups involving high stretch. In this study Dragon Skin 10 [40], [61] and Dragon Skin 30 have been evaluated using the Yeoh formulation. The Yeoh model remains a frequently selected option among hyperelastic formulations due to its high accuracy across different modes of loading. Its polynomial structure allows flexible stress-strain curve fitting across both linear and nonlinear strain ranges with reliable accuracy [40], [61], [62], [63], [64].

A. *MATHEMATICAL MODELING*

The bending behavior of the segmented actuator can be approximated by a simplified thin wall bending model is given by equation -1.

$$u(x) \approx \frac{P.R^2}{E_{eff}.t} \quad (1)$$

Where, $u(x)$ represents the actuator's displacement at a given point; P is the applied internal pressure; R is the characteristic radius of the actuator; $Eeff$ is the effective Young's modulus of the actuator material, reflecting its stiffness; and t is the wall thickness. Equation 1 serves as a practical guideline to quickly estimate how changes in pressure, geometry, or material properties will influence actuator displacement, supporting rapid prototyping and material selection in soft robotics applications. The equation 2 expresses the fundamental linear relationship between stress and strain in an elastic material.

$$\sigma = E_{eff} \cdot \varepsilon \quad (2)$$

where, σ denotes the stress applied to the material (Pa); E_{eff} represents the tangent modulus and ε is the strain.

Equation 3 is von Mises stress, and a scalar value used to predict yielding of ductile materials under complex loading conditions by combining the three principal stresses into a single equivalent stress. It simplifies complex stress states into a single value that can be directly compared with known material limits, facilitating safer and more efficient designs.

$$\sigma_v = \sqrt{\frac{1}{2}[(\sigma_1 - \sigma_2)^2 + (\sigma_2 - \sigma_3)^2 + (\sigma_3 - \sigma_1)^2} \quad (3)$$

The mathematical representation of the Yeoh model is expressed by the strain energy density function, which is given by equation 4:

$$W = C_1(I_1 - 3) + C_2(I_2 - 3)^2 + C_3(I_3 - 3)^3 \quad (4)$$

where

$$I_1 = \lambda_1^2 + \lambda_2^2 + \lambda_3^2 \quad (5)$$

$$I_2 = \lambda_1^2\lambda_2^2 + \lambda_2^2\lambda_3^2 + \lambda_3^2\lambda_1^2 \quad (6)$$

$$I_3 = \lambda_1^2\lambda_2^2\lambda_3^2 = J^2 \quad . \quad (7)$$

W is strain energy density function and incorporates materials, parameters, C_1, C_2, and C_3, along with the invariants of the right Cauchy-Green deformation tensor, I_1, I_2, and I_3. J is the is the Jacobian determinant, which equals to 1 for incompressible materials.

$$J = \lambda_1\lambda_2\lambda_3 = 1 \quad (8)$$

In the Yeoh model, the strain energy function depends solely on the first invariant I_1, which is

defined as the sum of squares of the principal stretch ratios. This choice assumes material incompressibility (I_3=1) and reduces computational complexity, making it suitable for modeling silicone elastomers such as Dragon Skin 10 and 30." The Yeoh model was selected to simulate large strain behavior of the elastomeric skins due to its capability of accurately capturing the non-linear response under deformation, with parameters C_1, C_2, C_3 tuned separately for Dragon Skin 10 and 30.

Table 2. Material constants of hyper elastic model of the soft actuator.

Soft Material	Hyper elastic Model	Material Constants
Dragon 10[21]	Yeoh Model	C1=36kpa C2= 0.25kpa C3 =0.023kpa
Dragon 30[21]	Yeoh Model	C1 = 114.88kpa C2= 0.126kpa

B. FINITE ELEMENT ANALYSIS

The bending behavior of the segmented actuator In this research, a finite element analysis was performed to predict the behavior of a CAD model. The analysis was performed using the Static Structural analysis type, to analyze the behavior of Dragon 10 and Dragon 30, the materials were subjected to same loads and boundary conditions. To model the material behavior, a hyper elastic material Yeoh model was employed, and the materials constants are presented in Table:3. A quadratic order type element with a size of 0.3m was utilized to perform a nonlinear mechanical analysis. To enhance the accuracy of the simulation outcomes, proximity capture was enabled for faces and edge elements. The resulting mesh is depicted in Figure 2 showing the details of the element distribution and the overall quality of the mesh. By using a quadratic order type element, a more precise representation of the mechanical behavior of the system was achieved. For this study, specific load and boundary conditions were applied to the pneumatic actuator. To ensure a stable system, a fixed support was applied at one end of the actuator. Additionally, pressure of 30kpa was introduced into the channels on the inner walls of the arm to simulate the pneumatic pressure. To further simulate real-world conditions, standard earth gravity of 9.806 m/s2 was applied in the negative Y direction. These load and boundary conditions are crucial in accurately representing the system's behavior under various operating conditions.

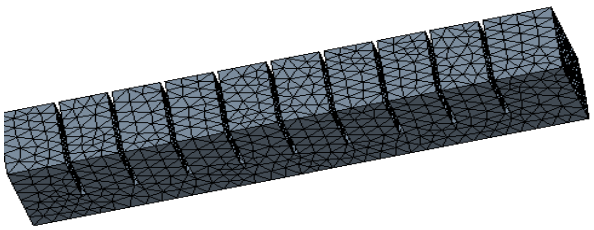

Figure 2. Meshing Configuration.

Table 3. Meshing Configuration.

Number of Nodes	Number of Elements
23357	13782

IV. RESULS AND DISCUSSION

The research paper describes the analysis of two different hyper elastic materials: Dragon 10 and Dragon 30 by using FEM-based. The analysis involves actuating two distinct soft actuators that were subjected to an actuating pressure of 30 kPa. This evaluation between Figure 3 and Figure 4 compares total deformation for the "Dragon 10" and "Dragon 30" skin models under equal boundary conditions and identical loading. The horizontal axis represents

spatial position along the actuator length; all distances are expressed in meters (m). The deformation magnitude is depicted using a continuous color scale; this scale also uses meters (m) as the unit. For both configurations, deformation starts from zero at the fixed left boundary; the value increases gradually toward the right free end of the model. A measurable difference is seen in the final deformation values; Dragon 10 shows a peak deformation of 0.161 m while Dragon 30 reaches only 0.092 m. This outcome confirms that Dragon 10 has a more flexible structure; its material and geometry allow greater deflection. In contrast, the Dragon 30 model responds with reduced displacement; this indicates its structure offers more resistance to deformation under the same applied force. The "Dragon 10 skin" has a larger bending angle than the "Dragon 30 skin." This is evident because its tip has deformed (moved) a greater distance, resulting in a tighter and more significant bend.

Table 4. Bending angle and Stress Distribution

Material	Max Deformation (m)	Max Strain	Max von Mises Stress (Pa)	Bending Angle (°)
Dragon 10	0.161	0.565	1.369×10^5	36°
Dragon 30	0.092	0.204	1.371×10^5	24°

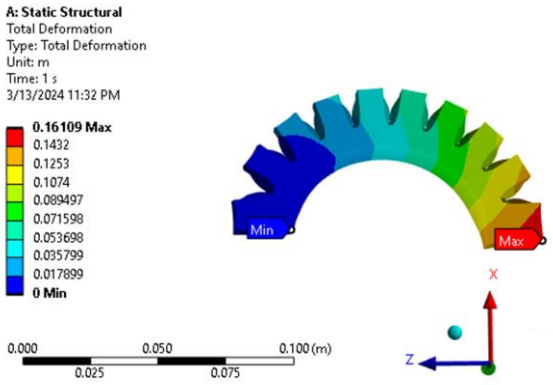

Figure 3. Dragon 10 skin total deformation

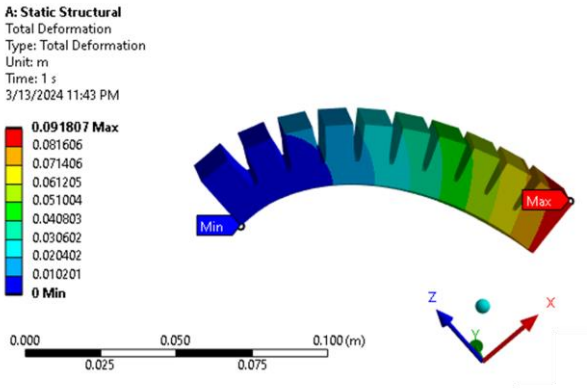

Figure 4. Dragon 30 skin total deformation

Figure 5 and Figure 6 compare Equivalent von-Mises Stress in the two actuator configurations under identical boundary conditions and similar mesh resolution. The horizontal axis indicates spatial length in meters (m); the vertical contour scale shows stress in Pascals (Pa). Stress is not spread evenly along either geometry; instead, it peaks at the inner arc near the fixed left boundary where the "Max" label appears. Stress gradually decreases toward the right end; this area is free of constraint and shows lower intensity.

Maximum values are close in magnitude for both models; Dragon 10 reaches 1.369 × 10^5 Pa while Dragon 30 peaks at 1.371 × 10^5 Pa. Though their structural compliance varies, both geometries guide load similarly; stress becomes focused at the same constrained zone near the base.

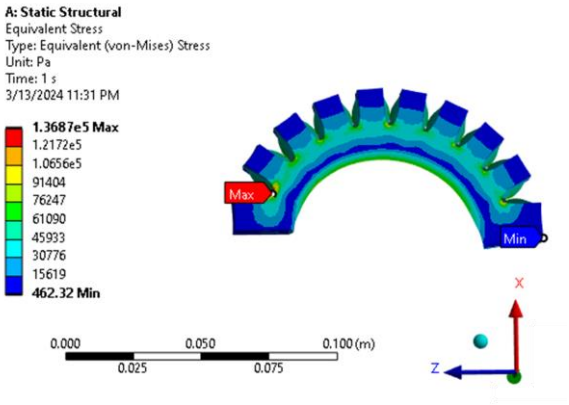

Figure – 5. Dragon 10 skin total stress

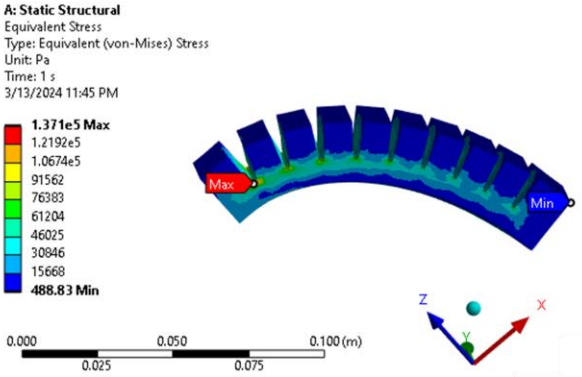

Figure 6. Dragon 30 skin total stress

The comparison between Figure 7 and Figure 8 evaluates Equivalent Elastic Strain across both configurations using the same load and boundary constraints for consistency. The horizontal axis defines spatial location in meters (m); the contour scale illustrates strain as a dimensionless ratio (m/m). The strain distribution pattern follows that of stress; the peak strain occurs at the inner curve of the first segment on the left fixed end. The Dragon 10 model records a maximum strain of 0.565; the Dragon 30 model reaches only 0.204 under identical conditions. These values align with earlier deformation outcomes; larger displacement has directly resulted in greater elastic strain. The higher strain in Dragon 10 indicates extensive local stretching; the Dragon 30 design restricts strain more effectively due to its stiffer geometry.

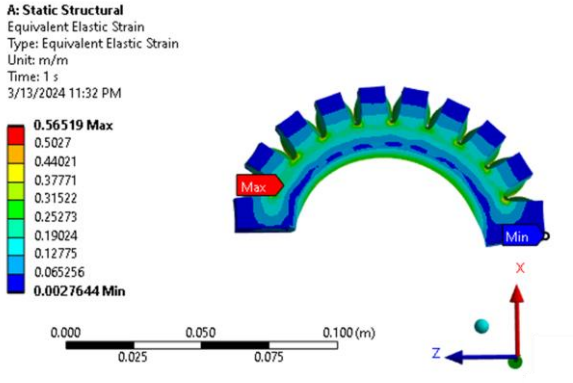

Figure 7. Dragon 10 skin total strain

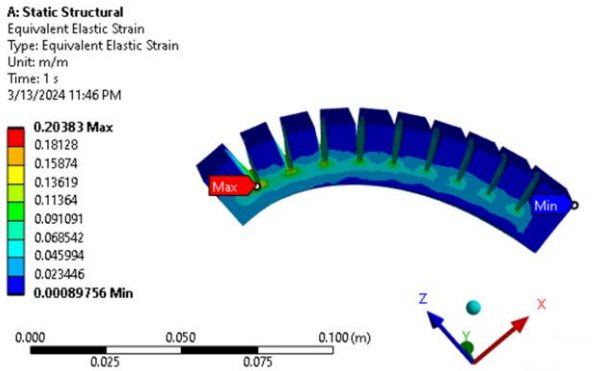

Figure 8. Dragon 30 skin total strain

This comparison between Figure 9 and Figure 10 investigates maximum structural deformation in response to applied pressure for the Dragon 10 and Dragon 30 skin models. The horizontal axis displays applied pressure in Pascals (Pa); the vertical axis indicates peak deformation in meters (m). For both models, the deformation rises non-linearly with pressure; the slope reduces gradually which shows a smaller deformation gain at higher loads. The primary distinction lies in output magnitude; at 30,000 Pa, Dragon 10 reaches approximately 0.16 m while Dragon 30 reaches only 0.09 m. Across the entire pressure range, Dragon 30 produces lower deformation; its geometry exhibits higher structural stiffness. This result confirms that the Dragon 10 skin remains more flexible under identical pressure levels when compared with the Dragon 30 configuration.

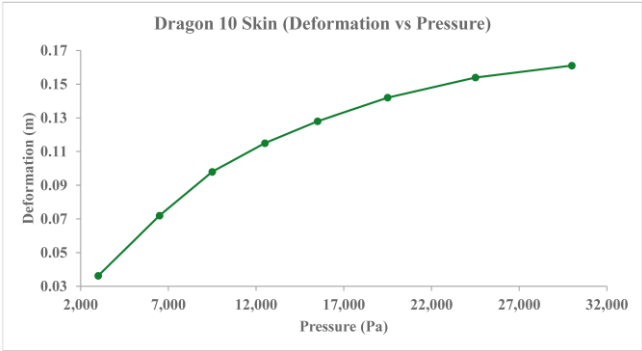

Figure 9. Dragon 10 Deformation vs. Pressure

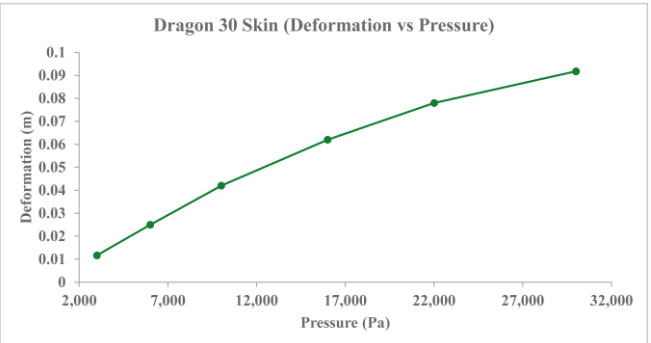

Figure 10. Dragon 30 Deformation vs. Pressure

Figure 11 and Figure 12 present the relation between maximum equivalent stress and applied pressure for both configurations. The horizontal axis denotes pressure in Pascals (Pa); the vertical axis indicates resulting stress in Pascals (Pa). A non-linear rise in stress is observed in both models; the stress growth rate declines as applied pressure increases. The plotted responses show extremely close agreement

between the two models; their curves follow almost the same trajectory across the full pressure range. Both designs register a peak stress of around 1.37 × 10^5 Pa at 30,000 Pa. This uniform outcome persists despite their large differences in stiffness and deformation. The load-bearing design in each structure causes stress levels to reach nearly the same maximum under identical pressure.

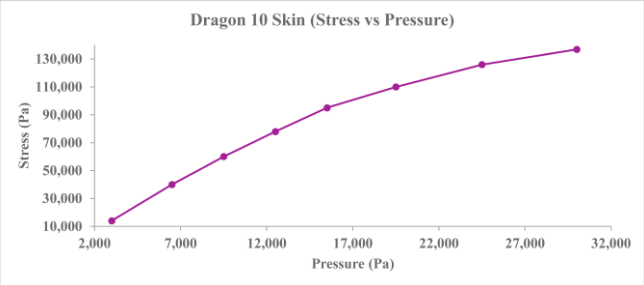

Figure 11. Dragon 10 Stress vs. Pressure

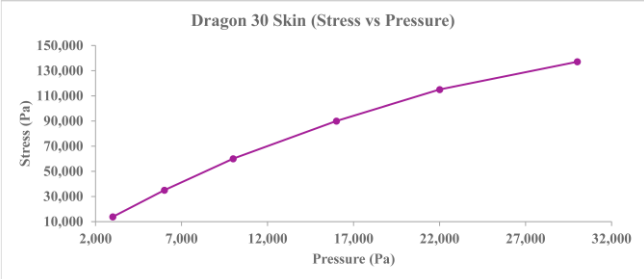

Figure 12. Dragon 30 Stress vs. Pressure

Figure 13 and Figure 14 display the stress-strain characteristics at the location where peak stress is recorded in the material. The horizontal axis shows strain in meters per meter (m/m); the vertical axis shows stress in Pascals (Pa). Both graphs represent a non-linear response; the slope of each curve reduces with increasing strain, indicating a

Figure 11 Dragon 10 Stress vs. Pressure drop in tangent modulus. Although both figures carry the label "Dragon 10 skin" the strain range confirms that Figure 14 corresponds to the Dragon 30 configuration. This interpretation aligns with the previously reported strain limit of 0.204 m/m. The same material model is used in both designs; however, the Dragon 10 model requires a much higher strain of 0.565 m/m to reach the maximum stress. The Dragon 30 structure reaches this same stress level with a lower strain of 0.204 m/m. These results show identical constitutive behavior but confirm that greater stiffness in the Dragon 30 model permits it to resist load with reduced strain.

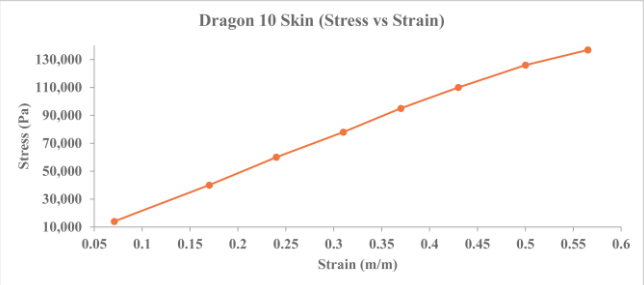

Figure 13. Dragon 10 Strain vs. Pressure

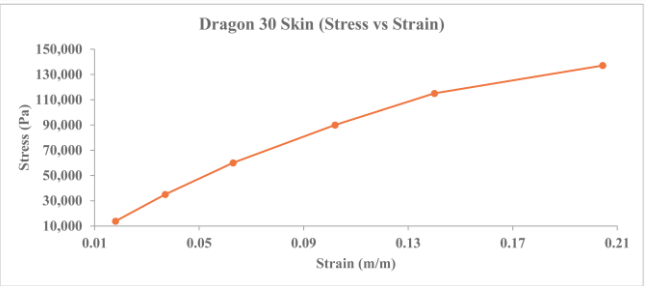

Figure 14. Dragon 30 Strain vs. Pressure

V. CONCULSION

The Finite Element Method was applied successfully to conduct a direct comparison between two elastomers used in soft pneumatic actuator construction; Dragon Skin 10 and Dragon Skin 30 were evaluated. This work addressed the common design compromise involving actuation efficiency and material durability; this trade-off was quantified through simulation results. The outcome confirmed that material choice strongly affects actuator behavior in predictable ways; softer materials produce higher deformation under equal loading conditions. Dragon Skin 10 demonstrated 75 percent greater maximum bending displacement; 0.161 meters was achieved compared to 0.092 meters for Dragon Skin 30 under identical pressures. This outcome supported its application in devices requiring high flexibility and range of motion; it proved more adaptable under deformation stress.

One essential finding concerned the separation of peak stress from material stiffness under the tested geometric and loading setup; both materials showed peak von Mises stress near 1.37 x 10^5 Pascals. This stress was concentrated around the inner curvature of the first chamber; the pressure and shape of the actuator governed stress distribution more than the compliance of the elastomer. Differences in deformation behavior became clearer in strain results; Dragon Skin 10 reached a peak equivalent strain of 0.565 while Dragon Skin 30 only reached 0.204. This represented a 177 percent increase in strain for the more compliant material; larger deformation was linked with increased material stretch closer to operational strain limits. The contrast reflected a clear design trade-off; flexibility gained through material compliance must be balanced against potential reductions in fatigue life and long-term stability.

From an applied design viewpoint, this comparative evaluation offered a structured reference for selecting elastomer properties that align with specific performance requirements. Dragon Skin 10 has shown better suitability in cases requiring high dexterity. Such cases include soft robotic grippers for handling delicate components and flexible mechanisms operating in limited or irregular environments where large displacement is required. Dragon Skin 30 has supported applications emphasizing sustained mechanical stability; its reduced strain capacity allows for increased safety margins during continuous use. This material has shown greater relevance for controlled-motion tasks such as assistive medical tools and automated assembly operations.

The investigation included known limitations; the analysis remained limited to static load conditions with no inclusion of time-dependent responses or dynamic deformation behaviors such as viscoelastic effects. The mechanical fatigue resulting from repeated pressurization cycles was excluded; the simulation framework focused only on a standard PneuNet-type actuator. Future work should extend to experimental fatigue testing under realistic cyclic strain ranges; these findings will help estimate operational durability. The modeling approach should also be applied to alternate actuator geometries and additional hyperelastic materials; this step will expand the relevance and robustness of the design method. Such additions can help engineers move from intuition-based choices toward simulations guided by predictive data; better actuator performance can be achieved by selecting the right elastomer for each task.

ACKNOWLEDGMENT

The authors express their sincere gratitude to the Department of Mechatronic Engineering at Mehran University of Engineering and Technology, Jamshoro for generously providing the computing resources essential for this research. We are deeply appreciative of the department's invaluable support and contributions.

REFERENCES

[1] O. Yasa *et al.*, "An Overview of Soft Robotics," *Annu. Rev. Control Robot. Auton. Syst.*, vol. 6, no. 1, pp. 1–29, May 2023, doi: 10.1146/annurev-control-062322-100607.

[2] M. W. Spong, "An Historical Perspective on the Control of Robotic Manipulators," *Annu. Rev. Control Robot. Auton. Syst.*, vol. 5, no. 1, pp. 1–31, May 2022, doi: 10.1146/annurev-control-042920-094829.

[3] W. Yu *et al.*, "A minimally designed soft crawling robot for robust locomotion in unstructured pipes," *Bioinspir. Biomim.*, vol. 17, no. 5, p. 056001, Sep. 2022, doi: 10.1088/1748-3190/ac7492.

[4] K. Wong, M. Stölzle, W. Xiao, C. Della Santina, D. Rus, and G. Zardini, "Contact-Aware Safety in Soft Robots Using High-Order Control Barrier and Lyapunov Functions," 2025, *arXiv*. doi: 10.48550/ARXIV.2505.03841.

[5] H. Rodrigue and J. Kim, "Soft actuators in surgical robotics: a state-of-the-art review," *Intell. Serv. Robot.*, vol. 17, no. 1, pp. 3–17, Jan. 2024, doi: 10.1007/s11370-023-00506-1.

[6] E. Bardi, M. Gandolla, F. Braghin, F. Resta, A. L. G. Pedrocchi, and E. Ambrosini, "Upper limb soft robotic wearable devices: a systematic review," *J. NeuroEngineering Rehabil.*, vol. 19, no. 1, Aug. 2022, doi: 10.1186/s12984-022-01065-9.

[7] M. Netzev, A. Angleraud, and R. Pieters, "Soft Robotic Gripper With Compliant Cell Stacks for Industrial Part Handling," *IEEE Robot. Autom. Lett.*, vol. 5, no. 4, pp. 6821–6828, Oct. 2020, doi: 10.1109/lra.2020.3020546.

[8] G. Picardi, M. Chellapurath, S. Iacoponi, S. Stefanni, C. Laschi, and M. Calisti, "Bioinspired underwater legged robot for seabed exploration with low environmental disturbance," *Sci. Robot.*, vol. 5, no. 42, May 2020, doi: 10.1126/scirobotics.aaz1012.

[9] O. Perera, R. Liyanapathirana, G. Gargiulo, and U. Gunawardana, "A Review of Soft Robotic Actuators and Their Applications in Bioengineering, with an Emphasis on HASEL Actuators' Future Potential," *Actuators*, vol. 13, no. 12, p. 524, Dec. 2024, doi: 10.3390/act13120524.

[10] N. El-Atab *et al.*, "Soft Actuators for Soft Robotic Applications: A Review," *Adv. Intell. Syst.*, vol. 2, no. 10, Oct. 2020, doi: 10.1002/aisy.202000128.

[11] M. S. Xavier *et al.*, "Soft Pneumatic Actuators: A Review of Design, Fabrication, Modeling, Sensing, Control and Applications," *IEEE Access*, vol. 10, pp. 59442–59485, 2022, doi: 10.1109/access.2022.3179589.

[12] A. Pagoli, F. Chapelle, J.-A. Corrales-Ramon, Y. Mezouar, and Y. Lapusta, "Review of soft fluidic actuators: classification and materials modeling analysis," *Smart Mater. Struct.*, vol. 31, no. 1, p. 013001, Jan. 2022, doi: 10.1088/1361-665x/ac383a.

[13] M. S. Xavier, A. J. Fleming, and Y. K. Yong, "Design and Control of Pneumatic Systems for Soft Robotics: A Simulation Approach," *IEEE Robot. Autom. Lett.*, vol. 6, no. 3, pp. 5800–5807, Jul. 2021, doi: 10.1109/lra.2021.3086425.

[14] N. Gariya, P. Kumar, and B. Prasad, "Stress and bending analysis of a soft pneumatic actuator considering different hyperelastic materials," *Mater. Today Proc.*, vol. 65, pp. 3126–3131, 2022, doi: 10.1016/j.matpr.2022.05.352.

[15] M. M. Durban *et al.*, "Custom 3D Printable Silicones with Tunable Stiffness," *Macromol. Rapid Commun.*, vol. 39, no. 4, Feb. 2018, doi: 10.1002/marc.201700563.

[16] H. B. Khaniki, M. H. Ghayesh, R. Chin, and M. Amabili, "A review on the nonlinear dynamics of hyperelastic structures," *Nonlinear Dyn.*, vol. 110, no. 2, pp. 963–994, Oct. 2022, doi: 10.1007/s11071-022-07700-3.

[17] Y. Ye, R. B. N. Scharff, S. Long, C. Han, and D. Du, "Modelling of soft fiber-reinforced bending actuators through transfer learning from a machine learning algorithm trained from FEM data," *Sens. Actuators Phys.*, vol. 368, p. 115095, Apr. 2024, doi: 10.1016/j.sna.2024.115095.

[18] C. Tawk and G. Alici, "Finite Element Modeling in the Design Process of 3D Printed Pneumatic Soft Actuators and Sensors," *Robotics*, vol. 9, no. 3, p. 52, Jul. 2020, doi: 10.3390/robotics9030052.

[19] L. Ding *et al.*, "Dynamic Finite Element Modeling and Simulation of Soft Robots," *Chin. J. Mech. Eng.*, vol. 35, no. 1, Dec. 2022, doi: 10.1186/s10033-022-00701-8.

[20] K. H. L. Heung, H. Li, Thomson. W. L. Wong, and S. S. M. Ng, "Assistive robotic hand with bi-directional soft actuator for hand impaired patients," *Front. Bioeng. Biotechnol.*, vol. 11, Jul. 2023, doi: 10.3389/fbioe.2023.1188996.

[21] L. Marechal, P. Balland, L. Lindenroth, F. Petrou, C. Kontovounisios, and F. Bello, "Toward a Common Framework and Database of Materials for Soft Robotics," *Soft Robot.*, vol. 8, no. 3, pp. 284–297, Jun. 2021, doi: 10.1089/soro.2019.0115.

[22] B. Hasanshahi, L. Cao, K.-Y. Song, and W. Zhang, "Design of Soft Robots: A Review of Methods and Future Opportunities for Research," *Machines*, vol. 12, no. 8, p. 527, Aug. 2024, doi: 10.3390/machines12080527.

[23] S. Mollaee, D. M. Budgett, A. J. Taberner, and P. M. F. Nielsen, "Hyperelastic constitutive model parameters identification using optical-based techniques and hybrid optimisation," *Int. J. Mech. Mater. Des.*, vol. 20, no. 2, pp. 233–249, Apr. 2024, doi: 10.1007/s10999-023-09673-6.

[24] H. B. Khaniki, M. H. Ghayesh, R. Chin, and M. Amabili, "Hyperelastic structures: A review on the mechanics and biomechanics," *Int. J. Non-Linear Mech.*, vol. 148, p. 104275, Jan. 2023, doi: 10.1016/j.ijnonlinmec.2022.104275.

[25] M. Destrade, G. Saccomandi, and I. Sgura, "Methodical fitting for mathematical models of rubber-like materials," *Proc. R. Soc. Math. Phys. Eng. Sci.*, vol. 473, no. 2198, p. 20160811, Feb. 2017, doi: 10.1098/rspa.2016.0811.

[26] S. S. Kulkarni, N. M. Bayre, and K. A. Khan, "Modelling visco-hyperelastic response of Silicone based elastomers for soft robotics and foldable structure applications," *Int. J. Eng. Sci.*, vol. 211, p. 104253, Jun. 2025, doi: 10.1016/j.ijengsci.2025.104253.

[27] Q. Xiong, B. W. K. Ang, T. Jin, J. W. Ambrose, and R. C. H. Yeow, "Earthworm-Inspired Multi-Material, Adaptive Strain-Limiting, Hybrid Actuators for Soft Robots," *Adv. Intell. Syst.*, vol. 5, no. 3, Mar. 2023, doi: 10.1002/aisy.202200346.

[28] M. Fatahillah, N. Oh, and H. Rodrigue, "A Novel Soft Bending Actuator Using Combined Positive and Negative Pressures," *Front. Bioeng. Biotechnol.*, vol. 8, May 2020, doi: 10.3389/fbioe.2020.00472.

[29] N. Gariya, P. Kumar, R. S. Bangari, and M. Makkar, "Bending analysis of a soft pneumatic actuator using analytical and numerical methods," *Mater. Today Proc.*, Jul. 2023, doi: 10.1016/j.matpr.2023.06.268.

[30] T. Wang, L. Ge, and G. Gu, "Programmable design of soft pneu-net actuators with oblique chambers can generate coupled bending and twisting motions," *Sens. Actuators Phys.*, vol. 271, pp. 131–138, Mar. 2018, doi: 10.1016/j.sna.2018.01.018.

[31] N. Gariya, P. Kumar, and T. Singh, "Experimental study on a bending type soft pneumatic actuator for minimizing the ballooning using chamber-reinforcement," *Heliyon*, vol. 9, no. 4, p. e14898, Apr. 2023, doi: 10.1016/j.heliyon.2023.e14898.

[32] K. Y. Volokh, "Modeling failure of soft anisotropic materials with application to arteries," *J. Mech. Behav. Biomed. Mater.*, vol. 4, no. 8, pp. 1582–1594, Nov. 2011, doi: 10.1016/j.jmbbm.2011.01.002.

[33] E. Ménager, T. Navez, P. Chaillou, O. Goury, A. Kruszewski, and C. Duriez, "Modeling, Embedded Control and Design of Soft Robots using a Learned Condensed FEM Model," 2025, *arXiv*. doi: 10.48550/ARXIV.2503.15009.

[34] N. Wang, B. Chen, X. Ge, X. Zhang, and W. Wang, "Modular crawling robots using soft pneumatic actuators," *Front. Mech. Eng.*, vol. 16, no. 1, pp. 163–175, Mar. 2021, doi: 10.1007/s11465-020-0605-3.

[35] M. Loepfe, C. M. Schumacher, U. B. Lustenberger, and W. J. Stark, "An Untethered, Jumping Roly-Poly Soft Robot Driven by Combustion," *Soft Robot.*, vol. 2, no. 1, pp. 33–41, Mar. 2015, doi: 10.1089/soro.2014.0021.

[36] S. Habibian, B. B. Wheatley, S. Bae, J. Shin, and K. W. Buffinton, "Evaluation of two complementary modeling approaches for fiber-reinforced soft actuators," *ROBOMECH J.*, vol. 9, no. 1, Dec. 2022, doi: 10.1186/s40648-022-00225-9.

[37] Z. Qiu *et al.*, "An empirical model of soft bellows actuator," *Sci. Rep.*, vol. 14, no. 1, Nov. 2024, doi: 10.1038/s41598-024-79084-w.

[38] T. Wu, Z. Liu, B. Wang, Z. Ma, D. Ma, and X. Deng, "A Versatile Topology-Optimized Compliant Actuator for Soft Robotic Gripper and Walking Robot," *Soft Robot.*, vol. 11, no. 1, pp. 157–170, Feb. 2024, doi: 10.1089/soro.2022.0247.

[39] G. Zhong, W. Dou, X. Zhang, and H. Yi, "Bending analysis and contact force modeling of soft pneumatic actuators with pleated structures," *Int. J. Mech. Sci.*, vol. 193, p. 106150, Mar. 2021, doi: 10.1016/j.ijmecsci.2020.106150.

[40] M. S. Xavier, A. J. Fleming, and Y. K. Yong, "Finite Element Modeling of Soft Fluidic Actuators: Overview and Recent Developments," *Adv. Intell. Syst.*, vol. 3, no. 2, Feb. 2021, doi: 10.1002/aisy.202000187.

[41] A. Sarker, T. Ul Islam, and Md. R. Islam, "A Review on Recent Trends of Bioinspired Soft Robotics: Actuators, Control Methods, Materials Selection, Sensors, Challenges, and Future Prospects," *Adv. Intell. Syst.*, vol. 7, no. 3, Mar. 2025, doi: 10.1002/aisy.202400414.

[42] Y. Chen *et al.*, "Bioinspired hydrogel actuator for soft robotics: Opportunity and challenges," *Nano Today*, vol. 49, p. 101764, Apr. 2023, doi: 10.1016/j.nantod.2023.101764.

[43] E. Porte, S. Eristoff, A. Agrawala, and R. Kramer-Bottiglio, "Characterization of Temperature and Humidity Dependence in Soft Elastomer Behavior," *Soft Robot.*, vol. 11, no. 1, pp. 118–130, Feb. 2024, doi: 10.1089/soro.2023.0004.

[44] H. J. Qi, K. Joyce, and M. C. Boyce, "Durometer Hardness and the Stress-Strain Behavior of Elastomeric Materials," *Rubber Chem. Technol.*, vol. 76, no. 2, pp. 419–435, May 2003, doi: 10.5254/1.3547752.

[45] P. D. H. Bui, B. Prugh, A. M. E. Padilla, C. Schell, M. Keller, and J. A. Schultz, "Endurance tests for a fabric_reinforced inflatable soft actuator," *Front. Mater.*, vol. 10, May 2023, doi: 10.3389/fmats.2023.1112540.

[46] L. Rupert, B. O. Saunders, and M. D. Killpack, "Performance Metrics for Fluidic Soft Robot Rotational Actuators," *Front. Robot. AI*, vol. 8, Aug. 2021, doi: 10.3389/frobt.2021.632835.

[47] M. Carton *et al.*, "Bridging hard and soft: Mechanical metamaterials enable rigid torque transmission in soft robots," *Sci. Robot.*, vol. 10, no. 100, Mar. 2025, doi: 10.1126/scirobotics.ads0548.

[48] Y. Qian, S. Han, G. Aguirre-Ollinger, C. Fu, and H. Yu, "Design, Modelling, and Control of a Reconfigurable Rotary Series Elastic Actuator with Nonlinear Stiffness for Assistive Robots," 2022, doi: 10.48550/ARXIV.2205.14412.

[49] L. Ge, T. Wang, N. Zhang, and G. Gu, "Fabrication of Soft Pneumatic Network Actuators with Oblique Chambers," *J. Vis. Exp.*, no. 138, Aug. 2018, doi: 10.3791/58277.

[50] P.-S. Lin, O. Le Roux De Bretagne, M. Grasso, J. Brighton, C. StLeger-Harris, and O. Carless, "Comparative Analysis of Various Hyperelastic Models and Element Types for Finite Element Analysis," *Designs*, vol. 7, no. 6, p. 135, Nov. 2023, doi: 10.3390/designs7060135.

[51] Y. Li, J. A. Ong, and P. S. Lee, "Two-dimensional materials for adaptive functionalities in soft robotics," *Mater. Horiz.*, 2025, doi: 10.1039/d5mh00565e.

[52] W.-T. Yang, H. Stuart, B. Kurkcu, and M. Tomizuka, "Nonlinear Modeling for Soft Pneumatic Actuators via Data-Driven Parameter Estimation," Feb. 14, 2024, *arXiv*: arXiv:2311.02527. doi: 10.48550/arXiv.2311.02527.

[53] C. Schaff, A. Sedal, and M. R. Walter, "Soft Robots Learn to Crawl: Jointly Optimizing Design and Control with Sim-to-Real Transfer," Feb. 09, 2022, *arXiv*: arXiv:2202.04575. doi: 10.48550/arXiv.2202.04575.

[54] A. M. Ţîţu, V. Gusan, M. Dragomir, A. B. Pop, and Ştefan Ţîţu, "Cost Calculation and Deployment Strategies for Collaborative Robots in Production Lines: An Innovative and Sustainable Perspective in Knowledge-Based Organizations," *Sustainability*, vol. 16, no. 13, p. 5292, Jun. 2024, doi: 10.3390/su16135292.

[55] M. R. Abdullah *et al.*, "Comprehensive review of 3D/4D printing of soft materials, methods and applications," *Appl. Mater. Today*, vol. 43, p. 102667, Apr. 2025, doi: 10.1016/j.apmt.2025.102667.

[56] T. Ashuri, A. Armani, R. Jalilzadeh Hamidi, T. Reasnor, S. Ahmadi, and K. Iqbal, "Biomedical soft robots: current status and perspective," *Biomed. Eng. Lett.*, vol. 10, no. 3, pp. 369–385, Aug. 2020, doi: 10.1007/s13534-020-00157-6.

[57] F. J. Tauber and V. Slesarenko, "Early career scientists converse on the future of soft robotics," *Front. Robot. AI*, vol. 10, Feb. 2023, doi: 10.3389/frobt.2023.1129827.

[58] M. T. Tolley *et al.*, "A Resilient, Untethered Soft Robot," *Soft Robot.*, vol. 1, no. 3, pp. 213–223, Sep. 2014, doi: 10.1089/soro.2014.0008.

[59] J. C. Case, E. L. White, and R. K. Kramer, "Soft Material Characterization for Robotic Applications," *Soft Robot.*, vol. 2, no. 2, pp. 80–87, Jun. 2015, doi: 10.1089/soro.2015.0002.

[60] Z. Wang, M. Zhu, S. Kawamura, and S. Hirai, "Comparison of different soft grippers for lunch box packaging," *Robot. Biomim.*, vol. 4, no. 1, Dec. 2017, doi: 10.1186/s40638-017-0067-1.

[61] M. Behroozi, O. A. Olatunbosun, and W. Ding, "Finite element analysis of aircraft tyre – Effect of model complexity on tyre performance characteristics," *Mater. Des.*, vol. 35, pp. 810–819, Mar. 2012, doi: 10.1016/j.matdes.2011.05.055.

[62] J. Wang, Y. Fei, and W. Pang, "Design, Modeling, and Testing of a Soft Pneumatic Glove With Segmented PneuNets Bending Actuators," *IEEEASME Trans. Mechatron.*, vol. 24, no. 3, pp. 990–1001, Jun. 2019, doi: 10.1109/tmech.2019.2911992.

[63] N. Elango, A. A. Mohd Faudzi, M. R. Muhammad Razif, and I. N. A. Mohd Nordin, "Determination of Non-Linear Material Constants of RTV Silicone Applied to a Soft Actuator for Robotic Applications," *Key Eng. Mater.*, vol. 594–595, pp. 1099–1104, Dec. 2013, doi: 10.4028/www.scientific.net/kem.594-595.1099.

[64] Y. Zhu, K. Chu, X. Chen, X. Wang, and H. Su, "Research and application of a multi-degree-of-freedom soft actuator," *Sens. Actuators Phys.*, vol. 338, p. 113492, May 2022, doi: 10.1016/j.sna.2022.113492.